Computer Model for Multipass Repair Welds in SA508 Class 2 Alloy

A computer model helps to automate GTAW repair welding in a nuclear reactor

BY P. J. ALBERRY

ABSTRACT. A predictive methodology for the calculation of heat-affected zone hardness distributions in thick-section multipass welds in SA508 Class 2 material is described. The methodology developed has been incorporated into a computer model that has been used to develop an alternative repair technique to the ASME XI "half-bead" technique. The alternative welding procedure identified by the model involves the deposition of six layers of weld metal using a mechanized gas tungsten arc welding (GTAW) process. Welding parameters identified for each layer produce successive refinement and tempering in the underlying heat-affected zone. Predicted hardness distributions are compared with hardness data taken from various six-layer welds together with predicted and measured hardness distributions for the ASME XI half-bead technique.

Introduction

In 1979, EPRI (Electric Power Research Institute) initiated a research contract EPRI-RP 1236 entitled "Repair Welding of Heavy Section Steel Nozzles," at Babcock and Wilcox, Alliance, Ohio. This project was designed to define and validate an alternative to the ASME XI half-bead repair procedure for boiling water reactor (BWR) nozzles. Both repair procedures are intended for use without postweld heat treatment. The half-bead procedure uses a layer-by-layer refinement and tempering technique and is carried out manually. Half of the first layer of weld metal is manually ground off to facilitate the refinement and tempering action of subsequent layers. The heavy dependence on time-consuming manual activities was considered to be a serious practical limitation in a BWR environment, due to the prolonged exposure to radioactivity. Consequently, the alternative technique was designed to be capable of mechanization.

A computer model for the GTAW process was used to facilitate the weld procedure development. This work was carried out in three phases. The first phase was to establish the basic welding metallurgy for SA508 Class 2 heat-affected zones (HAZ), and has already been reported (Ref. 1). The second phase, which is reported here, details the use of the computer model to develop a viable GTAW welding procedure. The third phase, a computer model sensitivity analysis of the likely variability of the ASME XI half-bead technique and alternative GTAW technique, will be reported shortly.

Computer Model

A detailed description of the computer model for the prediction of weld HAZ structures produced by the GTAW process has been produced by Alberry, Brunnstrom and Jones (Ref. 2).

Weld HAZ's in a given material consist of a range of structures that reflect the thermal cycles experienced. Thermal cycles with peak temperatures close to the melting point are experienced near the fusion boundary and usually result in the formation of coarse-grained structures. At greater distances from the fusion boundary, the thermal cycle peak temperatures decrease progressively and more fine-grained structures are formed.

KEY WORDS

Predicted Hardnesses
HAZ Hardness
Hardness Distribution
Computer Model
GTA Repair Technique
SA508 Class 2 Steel
Six Layer GTA Welds
Welding Parameters
Thick Section Welds
Multipass GTA Welds

Eventually the thermal cycle peak temperature decreases below the Ac_1 and the base material structure is only tempered. This basic unit for a single weld bead is shown in Fig. 1.

In multipass welds, the HAZ formed by the deposition of a single weld bead can be modified by the superposition of successive adjacent weld bead deposits. The second thermal cycle modifies the structure of the primary HAZ. Consequently, in the HAZ, the thermal cycles experienced at different positions will vary widely, depending on distance from the fusion boundary.

The microstructure and properties at any given position in the HAZ will be determined by its thermal history, grain growth kinetics, phase transformation and tempering behavior. The thermal history will depend upon the welding conditions, joint geometry, the weld bead shape, the spatial positioning of the weld beads and the resultant overlap of their HAZ's. The phase transformation and tempering behavior will be determined by chemical composition, prior structure, the austenite grain growth kinetics, the peak austenitizing temperature and the heating and cooling rates during the thermal cycle experienced.

Thus, to define the structure and hence infer the properties obtained in the HAZ of a given material composition, it is necessary to describe:

1) Weld bead shape.
2) The thermal cycle as a function of welding procedure in all regions of the HAZ.
3) Prior austenite grain growth as a function of prior structure and weld thermal cycle.
4) Transformation behavior as a function of thermal cycle and prior austenite grain size.
5) Tempering effects as a function of thermal cycle experienced by a given transformation product.

Elements 3–5 have been characterized in detail for SA508 Class 2 (Ref 1).

The thermal history can be calculated from standard heat-flow equations, but

P. J. ALBERRY is with Marchwood Engineering Laboratories, Central Electricity Generating Board, Marchwood, Southampton, U.K.

the position of the fusion boundary cannot be calculated accurately. To overcome this, the weld bead dimensions are established for a given range of welding conditions and the measured position of the fusion boundary is used as a reference point for the heat-flow calculations. The HAZ isotherms are thus calculated relative to the known position of the fusion boundary. This ensures that the heat-flow calculations are carried out in that region of the HAZ where conductive heat transfer dominates. This provides a better estimate of the spatial position of the fusion boundary and associated HAZ relative to the plate surface than would be achieved using point-source heat-flow calculations alone.

The following sections describe the empirical measurement of weld bead shape carried out by Babcock and Wilcox, some multiple thermal cycle weld simulation experiments carried out to validate the algorithms used for hardness prediction, and the calculation of a potential repair procedure and its subsequent practical validation.

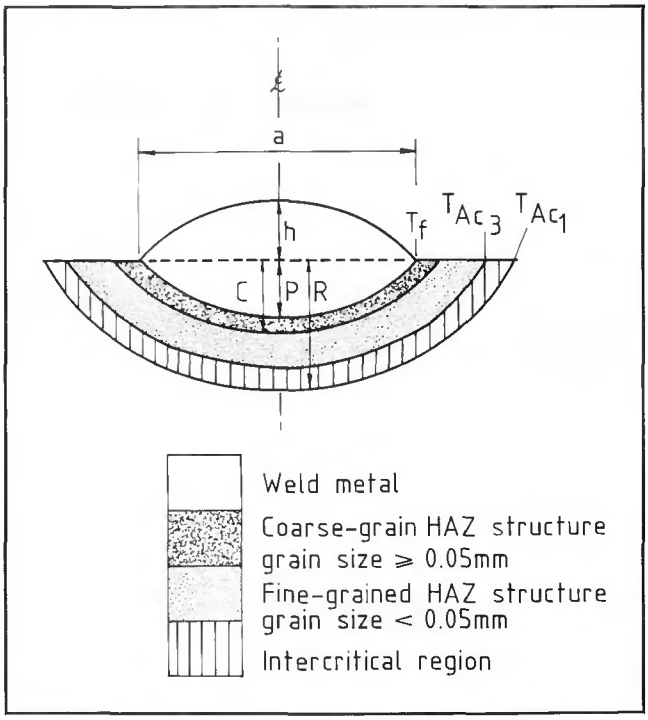

Fig. 1—Schematic single weld bead and HAZ structure

Experiments and Results

Weld Bead Shape Measurements

A series of ten weld beads were deposited using the GTAW process on SA508 Class 2 base plate. The base plate composition and welding conditions used are given in Tables 1 and 2. The welds were sectioned, polished and etched in 2% nital—Fig. 2. Weld bead width, height, central joint penetration and distance from the fusion boundary to the Ac_1 isotherm were measured. These values are given in Table 3.

Table 1—SA508 Class 2 Material Compositions (wt-%)

Element	Base Plate and Weld Simulation Specimens Single and Double Cycles	Furnace Tempering Specimens
C	0.23	0.24
Mn	0.62	0.61
P	0.010	0.017
S	0.018	0.010
Si	0.17	0.31
Ni	0.95	0.93
Cr	0.28	0.39
Mo	0.70	0.72
V	0.01	0.025
Nb	0.01	0.013
Al	0.017	0.015
Ti	0.01	0.01
B	0.001	–
Cu	0.062	0.073
Sn	0.015	0.023
As	0.020	0.040
Sb	–	<0.01

Weld Simulation

Weld simulation specimens, 200 mm long (8 in.) and 9 mm (0.4 in.) in diameter, were machined from a block, 130 × 75 × 75 mm (5 × 3 × 3 in.), of SA508 Class 2. Weld simulation techniques (Refs. 1, 3), using a machine similar to a Gleeble, were used to cycle a series of 14 specimens through a range of double weld thermal cycles corresponding to a multipass weld. The first thermal cycle for each specimen was chosen with a peak temperature of 1300°C (2372°F), to reproduce the coarse-grained HAZ region of a single weld bead (Ref. 1)—Table 4. Each specimen was then subjected to a second thermal cycle each with a different peak temperature designed to produce a range of retransformation and tempering effects that would be caused by the deposition of adjacent weld beads during welding. High-speed dilatometric measurements, with a sampling frequency of 10 Hz, were carried out during the heating and cooling portions of each weld thermal cycle.

Diametral strain and temperature were logged automatically using a Hewlett Packard 9825 minicomputer. Data plots of temperature versus strain were produced for each thermal cycle in the series and for each peak temperature selected. The percentage phase transformation was determined from the deviation from linearity of the temperature-to-strain plots assuming that the percentage transformation was proportional to diametral strain. Specimens were sectioned longitudinally and the Vickers diamond pyramid hardness (Hv) was measured at a load of 10 kg (Hv 10 kg) at the center of each specimen. These values are given in Table 5 and the hardness measurements from single weld thermal cycles (Ref. 1) are included in Table 4. Note that Vickers

Table 2—GTAW Welding Conditions[a]

Weld Bead	Current A	Voltage V	Travel Speed mm/s	Wire Feed Speed[b] mm/s	Preheat °C
1	200	11.0	2.54	31.3	21
2	220	11.0	2.54	31.3	21
3	220	11.0	2.96	31.3	21
4	220	11.0	3.39	31.3	21
5	220	11.0	3.51	31.3	21
6	135	9.0	2.54	10.6	100
7	160	10.0	2.54	12.7	100
8	190	10.0	2.54	16.9	100
9	180	9.5	1.52	27.5	200
10	180	9.5	1.52	27.5	300

(a) Ref. 10.
(b) Wire Type E70S1B, 0.89-mm diameter.

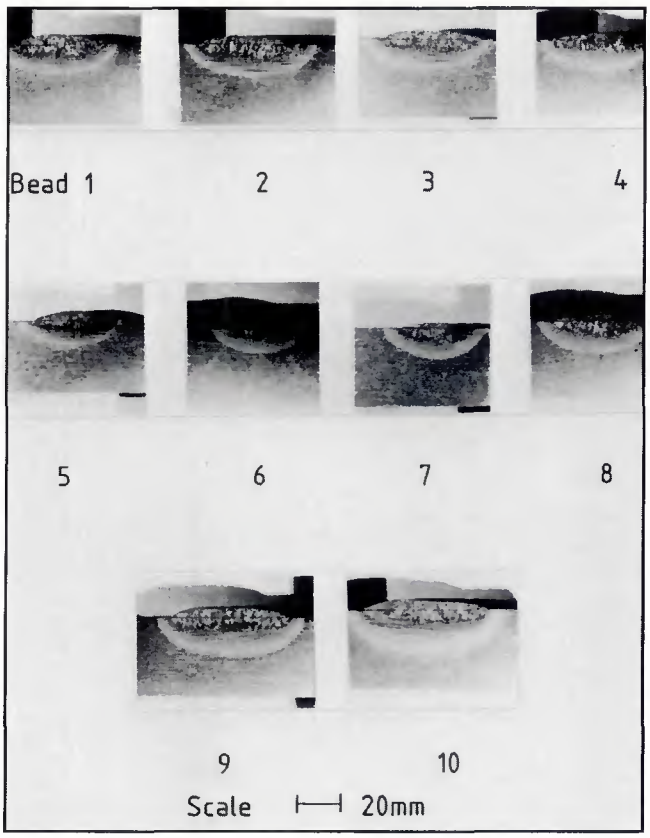

Fig. 2—Mechanized GTAW single weld bead deposits on SA508 Class 2 material (Ref. 10)

diamond pyramid hardness and Knoop diamond hardness are equivalent. An approximate conversion to the Rockwell C scale can be obtained by dividing the Vickers hardness value by a factor of 10.

Computer Model Algorithms

The computer model requires a series of algorithms for the calculation of weld bead dimensions, HAZ isotherms, the HAZ hardness of the appropriate transformation product and the tempering effects of those thermal cycles that do not cause retransformation. These algorithms are described in the following sections, and their validity is tested against experimental measurements.

Weld Bead Dimensions

Bead Width and Joint Penetration

The computer model requires algorithms for weld bead width and weld bead central joint penetration. These are shown in Fig. 3 plotted with gross heat input = VIv^{-1} where V is the welding voltage, I is the welding current and v is the travel speed.

Straight-line relationships were obtained using a least squares regression analysis and are shown together with the 95% confidence limits about the points:

mean bead width = 0.0077 (gross heat input) + 3.54; r = 0.95 (1)

mean penetration = −0.0002 (gross heat input) + 1.48; r = −0.13 (2)

where r is the correlation coefficient.

The observed straight-line relationships are entirely empirical, valid over the range of existing data, and have no physical or theoretical basis; they are used for computational convenience. They imply that the weld bead dimensions are constant along the length of a single bead and do not vary from bead to bead. Since this is unrealistic, a measure of the weld bead variability can be input to the model using a randomized value selected from the scatter about each of the straight lines shown in Fig. 3, where the distance between the 95% confidence limits represents four standard deviations.

Bead Height

Since the GTAW process used was continuously wire fed, the weld bead height cannot be calculated exclusively from the gross heat input. It is assumed that all the wire is melted and deposited on the plate surface with little spatter and that the top surface of the weld bead can be represented by the arc of a circle. This has previously been shown to be a good approximation for gross heat inputs in the range of 522–1825 J/mm (21–72 J/in.), a range of wire feed speeds of 11–19 mm/s (0.4–0.75 in./s) with a wire diameter of 1.2 mm (0.045 in.) and travel speeds in the range 1.7–4.2 mm/s^2. However, these assumptions will also be tested here. It can be shown that:

Table 3—Measured Weld Bead Dimensions

Weld Bead	Bead Width mm	Bead Height mm	Central Joint Penetration mm	Distance from Fusion Boundary AC_1 mm	Calculated Value of Arc[a] Efficiency η
1	9.91	1.17	1.40	2.00	1.18
2	11.20	1.05	1.91	2.19	1.24
3	10.41	0.95	1.27	2.33	1.61
4	9.91	0.89	1.14	1.89	1.22
5	8.38	1.00	1.27	1.85	1.22
6	7.37	0.50	1.14	1.61	1.15
7	7.62	0.60	1.52	1.95	1.22
8	9.02	0.65	1.65	2.00	1.11
9	11.9	1.20	1.00	3.33	1.46
10[b]	12.1	1.40	1.05	3.57	1.16

(a) This value is required to predict the fusion boundary. Ac_1 distance and is not strictly an arc efficiency that cannot have a value greater than unity. The average value of η is 1.25, with a standard deviation of 0.17. It is required for convenience as a curve-fitting parameter to produce an empirical fit to the observed data.
(b) Erratic bead, average of two sections.

Table 4—Weld Simulation Hardness Measurements[a]

Single Weld Thermal Cycle[b]	Vickers Hardness Hv 10 kg	Prior Austenite Grain Size mm
1300	468	0.100
1200	471	0.080
1100	449	0.040
1050	341	0.030
1000	357[c]	0.015
950	303	<0.015
900	267	<0.015
850	239	<0.015
800	238	~0.02 (Base Plate)
700	202	~0.02 (Base Plate)

(a) Ref. 1.
(b) The nomenclature refers to a weld thermal cycle with heating and cooling rates resulting from a heat input of 1 kJ/mm and a preheat of 100°C with the given weld thermal cycle peak temperature.
(c) This value differs from Alberry and Lambert (Ref. 1) because additional measurements have been included.

$$\frac{\pi\,(WD)^2 WFS}{4v} = 2\left(\left(\frac{\pi}{360}\left(\frac{h}{2}+\frac{a^2}{8h}\right)^2 \sin^{-1}\left(\frac{4ha}{4h^2+a^2}\right)\right)-\left(\frac{a^3}{32h}-\frac{ha}{8}\right)\right) \quad (3)$$

where WD is the wire diameter, WFS is the wire feed speed, h is the randomized weld bead height and a is the randomized bead width – Fig. 1.

Calculated values of bead height are shown in Fig. 4 plotted against the measured values. The agreement between the predicted and measured values is reasonable.

HAZ Dimensions

Previous workers (Refs. 4–6) have shown that a knowledge of the weld thermal cycle can be used to predict the rapid austenite grain growth that occurs in the HAZ's of low-alloy ferritic steels. The final grain size is given by an equation of the form:

$$D = \left(\Sigma_{t_{T_s}}^{t_{T_f}} A \exp - \frac{Q_{App}}{RT(t)}\Delta_t\right)^{\frac{1}{n}} \quad (4)$$

where t_{T_f} is the time at which transformation to austenite starts, t_{T_s} is the time at which transformation from austenite to the ferritic transformation product is completed during the cooling period of the cycle and all grain growth ceases, Q_{App} is the apparent activation energy for the grain growth process, A and n are constants over the experimental range of conditions, Δ_t is a time step used for numerical integration, R is the gas constant, and T(t) is the instantaneous temperature in K.

In the methods used to evaluate Q_{App}, A and n have been described (Ref. 4). Basic metallurgical constants for SA508 Class 2 are given in Table 6 (Ref. 1). T(t) is evaluated from a three-dimensional heat-flow equation for thick plate (Ref. 7):

$$T(t) = T_o + \frac{\phi}{2k\Theta R^1} \exp(-\lambda v\xi)\exp(-\lambda v R^1) \quad (5)$$

for a surface point source moving with constant velocity, v, along the x axis of a fixed rectangular coordinate (x,y,z) system.

T_o is the initial (preheat) temperature, K, k is the thermal conductivity, Θ is the solid angle in radians for the heat conduction path, $0.5\,\lambda^{-1}$ is the thermal diffusivity, and $\xi = x - vt$, where it is time. $R^1 = \sqrt{\xi^2 + y^2 + z^2}$ where ϕ is the arc power defined as ηVI, V and I are the welding voltage and current, and η is the arc efficiency, which depends upon the welding process (Refs. 8, 9).

The value of η in this investigation has been determined empirically from the measurements of the weld bead dimensions given in Table 3. Since the position of the fusion boundary is measured, the HAZ can be accurately described if the heat-flow model correctly predicts the distance from the fusion boundary to the Ac_1 isotherm. Values of η, which correctly predict measured fusion boundary Ac_1 distances, are shown in Table 3. The average value at the centerline of the

Table 5—Weld Simulation Hardness Measurements[a]

Double Weld Thermal Cycle[b]	Measured Vickers Hardness HV 10 kg	Measured % Transformation on Second Cycle	Calculated Vickers Hardness Hv 10 kg
1300; 1300	461	100	470
1300; 1200	464	100	469
1300; 1100	451	100	463
1300; 1000	455	100	456
1300; 900	426	100	450
1300; 880	443	86	441
1300; 860	390	62	402
1300; 840	354	38	371
1300; 800	315	0	322
1300; 750	318	0	343
1300; 700	349	0	365
1300; 650	349	0	384
1300; 600	388	0	401
1300; 550	405	0	415
1300; 500	424	0	424

(a) Ref. 1.
(b) The nomenclature refers to a weld thermal cycle with heating and cooling rates resulting from a heat input of 1kJ/mm and a preheat of 100°C with the given weld thermal cycle peak temperature.

Table 6—Basic Welding Metallurgy of SA508 Class 2 Heat-Affected Zones

Dynamic Ac_1	808°C
Dynamic Ac_3	892°C
Grain growth constant	2.1×10^{12} $mm^{1.3}s^{-1}$
Grain growth activation energy	460 kJ $mole^{-1}$
Grain growth exponent	1.3

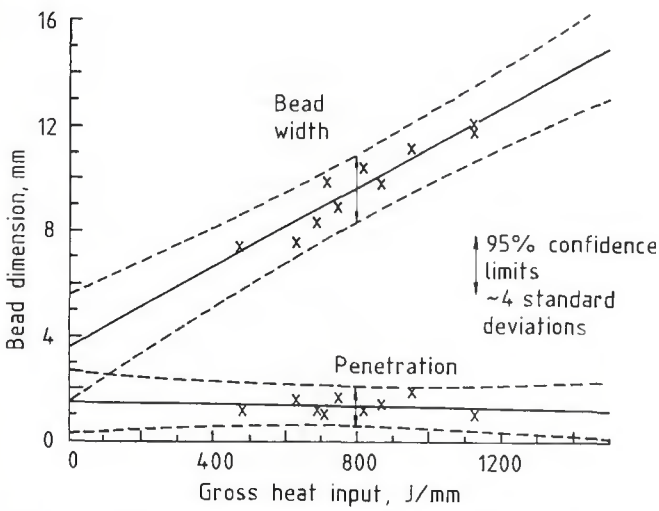

Fig. 3 – GTAW weld bead dimensions versus gross heat input

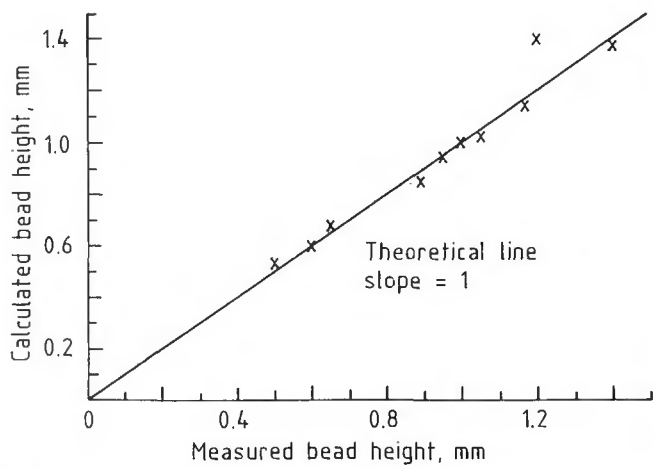

Fig. 4 – Comparison of calculated and measured weld bead heights

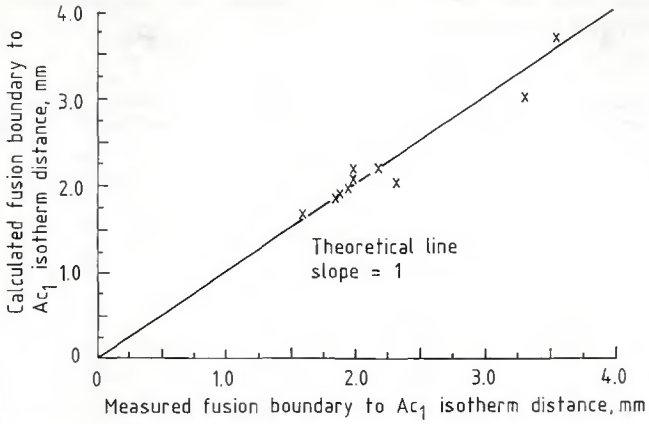

Fig. 5 — Comparison of calculated and measured fusion boundary to Ac_1

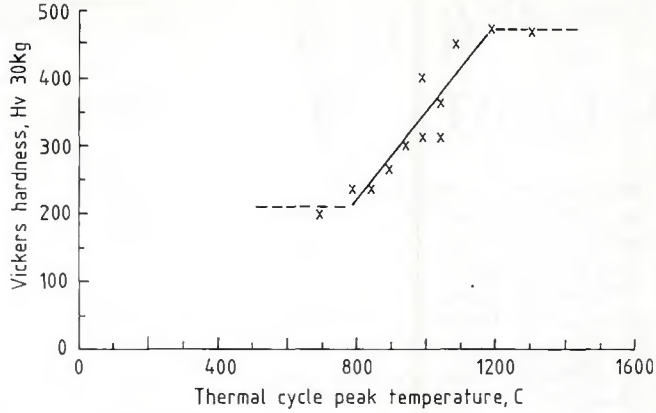

Fig. 6 — Measured HAZ hardness after a single weld thermal cycle

weld pool is 1.25. This does not imply an overall arc efficiency of 1.25, which is clearly impossible, but represents a local value that provides a best fit to the experimental data. The positions of all other isotherms are then calculated relative to the position of these two using the average value of η. Since weld beads are known to be inherently variable, the use of a single value of η can only be approximate. The fusion boundary to the Ac_1 isotherm distances calculated using the average value of η are compared with the measured values in Fig. 5, showing that the approximation is reasonable.

Algorithms for Prediction of HAZ Hardness Resulting from Phase Transformations

Single GTAW weld thermal cycles with high peak temperatures produced coarse-grained martensite, or coarse-grained martensite and lower bainite mixtures, which correspond closely to the microstructures observed at the fusion boundary of the weld HAZ's (Ref. 1). Weld thermal cycles with lower peak temperatures produce finer-grained microstructures, the prior austenite grain size decreasing with peak temperature. Thermal cycles with peak temperatures in the range ~800°-900°C (1472°-1652°F) produce various degrees of reaustenitization, resulting in intercritical structures. that are representative of those at the HAZ-base metal interface.

The decrease in grain size with thermal cycle peak temperature causes a shift in the continuous cooling transformation curve, which promotes the formation of higher temperature transformation products at a given cooling rate. A given weld HAZ could contain martensitic transformation products at the fusion boundary changing progressively to lower bainite, upper bainite and ferrite as the grain size decreases at increasing distances away from the fusion boundary. Some basic metallurgical constants for SA508 Class 2 are given in Table 6. In this material, even HAZ's adjacent to a single weld bead will contain a range of grain sizes and transformation structures that will have characteristics as-welded hardnesses. The actual HAZ hardness produced depends on the separate contributions from those elements taken into solid solution, the grain size, the carbide distribution, the transformation product and dislocation density. These effects are taken account of empirically using the algorithms described in the following section.

As-Welded HAZ Hardness Algorithms for Single Weld Thermal Cycles Derived from Weld Simulation Specimen Measurements

Various algorithms are required to calculate the as-welded HAZ hardness values as a function of position in the weld HAZ. Initially, the HAZ hardness produced by the deposition of a single weld bead is required. This can be calculated by first using the heat-flow equation to calculate the weld thermal cycle and using the weld thermal cycle to calculate the prior austenite grain size (Equation 4). This determines the transformation product on cooling for which the appropriate HAZ hardness has been measured from weld simulation specimens as a function of thermal cycle peak temperature — Table 4. These values are plotted in Fig. 6. The as-welded initial hardness distribution can be represented by the following algorithms:

$$T < Ac_1;\ Hv = 202 \quad (6)$$
$$Ac_1 < T < 1200;\ Hv = 0.633T - 290 \quad (7)$$
$$T > 1200;\ Hv = 470 \quad (8)$$

Equation 7 was obtained by least squares regression and has a correlation coefficient of 0.91. The equation has no known theoretical basis and is used for computational convenience.

Table 7 shows a comparison of measured weld simulated and weld HAZ hardnesses from different regions of the HAZ corresponding to coarse, medium, fine, very fine and intercritical prior austenite grain sizes. The values are in reasonable agreement, which reflects the accurate weld simulation of the transformation products and the precipitate distribution present in weld HAZs.

As-Welded Hardness Calculations for Multipass HAZ's Derived from Weld Simulation Specimen Measurements

Multipass weld HAZ's are more complex than single pass weld HAZ's. They experience multiple weld thermal cycles with peak temperatures ranging between the melting point and the preheat temperature. These thermal cycles can change the transformation product or temper the HAZ structure or leave the structure basically unaltered, depending on the peak temperature experienced and the cooling rate. The two basic mechanisms responsible for these changes are carbide dissolution and precipitation and grain growth while the material is austenitic.

Austenite is grain boundary nucleated on heating so that the grain growth process is repeated for each weld thermal cycle as soon as transformation to austenite on heating is complete. In low-alloy ferritic steels, grain growth is usually inhibited after transformation to a ferritic product on cooling. The presence of a stable precipitate distribution in the austenite can inhibit grain growth and some inhibition may also occur during the early stages of carbide dissolution on heating. However, carbide dissolution is rapid and complete by 1200°C (2192°F). Thus, the final prior austenite grain size achieved is largely characteristic of the last thermal cycle experienced if the peak temperature experienced exceeds 1200°C. Thus, the HAZ hardness produced for a double or multiple retransformation is given by the algorithms

$$Ac_3 < T < 1200;\ Hv = 0.067(T - Ac_3) + 449 \quad (9)$$
$$T > 1200;\ Hv = 470 \quad (10)$$

where T is the peak temperature of the

last thermal cycle. Note that for multiple thermal cycles, at least one of the previous thermal cycle peak temperatures is required to exceed 1200°C.

If all the weld thermal cycle peak temperatures experienced are less than 1100°C, the HAZ hardness may be derived from the single cycle algorithm (Equation 7).

This last assumption clearly underestimates the hardness since multiple thermal cycles in the range Ac_3–1100°C will progressively dissolve the carbides, eventually producing a hardened condition. This is discussed further in another section.

Algorithms for Prediction of HAZ Hardness Resulting from Tempering Effects Derived from Furnace Heat Treatment Specimens

The tempering curves for a range of HAZ structures were determined (Ref. 1) by furnace treatment of samples produced by weld thermal cycle peak temperatures of 1300°, 1200°, 1100°, 1050° and 1000°C (2390°, 2192°, 2012°, 1922° and 1832°F). Each specimen was tempered in a furnace for 0.5 h at temperatures of 300°, 400°, 500°, 600°, 650° and 700°C (752°, 932°, 1112°, 1202° and 1292°F). Three separate Vickers hardness determinations were carried out on each specimen. For each of the microstructural conditions, the tempering results were plotted against the Larson-Miller parameter (LMP) defined as

$$(1.8T + 492)(20 + \log t) \qquad (11)$$

where T is the temperature in °C and t is the time in hours.

These results are shown in Fig. 7. The hardness results were fitted to parabolic equations using a regression technique that produced the following algorithms for HAZ's. Note that the results for specimens that had experienced weld thermal cycle peak temperatures above 1100°C were indistinguishable and have been combined to produce a single algorithm.

peak temperature > 1100°C:

$$Hv = 435 + 8.0 \times 10^{-3} (LMP) - 3.6 \times 10^{-7} (LMP)^2 \qquad (12)$$

peak temperature 1000°–1100°C:

$$Hv = 372 + 6.1 \times 10^{-3} (LMP) - 2.6 \times 10^{-7} (LMP)^2 \qquad (13)$$

peak temperature < 1000°C:

$$Hv = 311 + 4.0 \times 10^{-3} (LMP) - 1.8 \times 10^{-7} (LMP)^2 \qquad (14)$$

The use of only three HAZ conditions is a major assumption that will be examined further in another section of the paper.

The HAZ hardness of a multipass weld deposit is determined by the particular combination of weld thermal cycles experienced at a given position in the weld HAZ. The initial cycles can produce hard, intermediate or soft starting structures that can then be progressively tempered by the action of various lower peak temperature weld thermal cycles, which do not produce a retransformation. The HAZ hardness produced after a tempering weld thermal cycle can be calculated using Equations 15 to 17. First, the Larson-Miller parameter for the weld thermal cycle is calculated by numerical integration. Effectively, this is done by dividing the weld thermal cycle into a large number of discontinuous isothermal steps such that the time interval for each step is short with respect to the weld thermal cycle. The Larson-Miller parameter for the arbitrary temperature and time interval is:

$$(1.8\,T(t) + 492)\,(20 + \log \Delta t) \qquad (15)$$

where T(t) represents the time dependence of the weld thermal cycle and Δt is the time step for numerical integration, taken as 0.1 s.

However, it is not possible to summate individual Larson-Miller parameters for each time interval. It is necessary to select an arbitrary normalizing temperature, chosen as 800°C in this case. Each Larson-Miller parameter is converted into an equivalent time at 800°C (1472°F), t_i^{800}, and the equivalent times summated for each isothermal step across the weld thermal cycle. The equivalent time at 800°C for the weld thermal cycle is given by:

$$\log (\Sigma_i\, t_i^{800}) = \Sigma_i \left[\frac{(1.8T(t)_i + 492)\,(20 + \log \Delta t)}{1932} - 20 \right] \qquad (16)$$

The constant, 1932, arises from the choice of 800°C as the normalizing temperature. The Larson-Miller parameter for the weld thermal cycle is then obtained from the equation,

$$LMP = (1932)\,(20 + \log \Sigma_i t_i^{800}) \qquad (17)$$

Table 7—Comparison of As-Welded Hardness Values for Single Weld Beads and Weld Simulation Specimens[a]

Weld HAZ Hardness Hv 10 kg	Weld Simulation Hardness Hv 10 kg	Grain Size in HAZ
455	450–471	Coarse
450	400–450	Medium
350	311–375	Fine
275	267	Very fine
225	238	Intercritical

(a) Ref. 1.

The tempering effects can then be estimated by substituting the calculated Larson-Miller value for the weld thermal cycle into Equations 12 to 14.

Algorithms for Prediction of HAZ Hardness Resulting from Partial Retransformation

Prior sections have dealt with the HAZ hardness produced from transformation effects for single and multiple thermal cycles and the tempering of each of the possible as-transformed structures. However, regions of the HAZ that experience weld thermal cycles with peak temperatures between the Ac_1 and Ac_3 are only partially transformed. The resultant HAZ hardness can be estimated from a knowledge of the fraction transformed as a function of peak temperature. Table 5 shows that the percentage transformation is approximately linear, with peak temperature between the Ac_1 and Ac_3. That fraction of the HAZ that is retransformed is given the HAZ hardness appropriate to the condition as described by Equation 7, if the previous cycles had not exceeded 1100°C. If the previous weld thermal cycle peak temperature had exceeded 1100°C, then the simplifying assumption made is that the hardness of all transformed regions that experience peak temperatures in the range Ac_1–Ac_3 will have HAZ hardnesses approximately

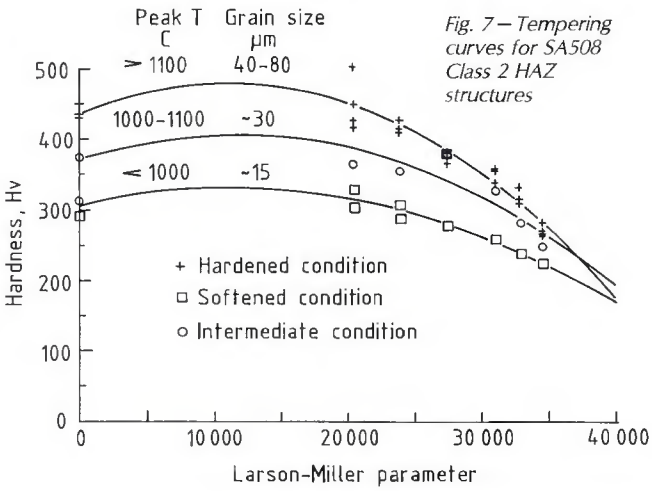

Fig. 7—Tempering curves for SA508 Class 2 HAZ structures

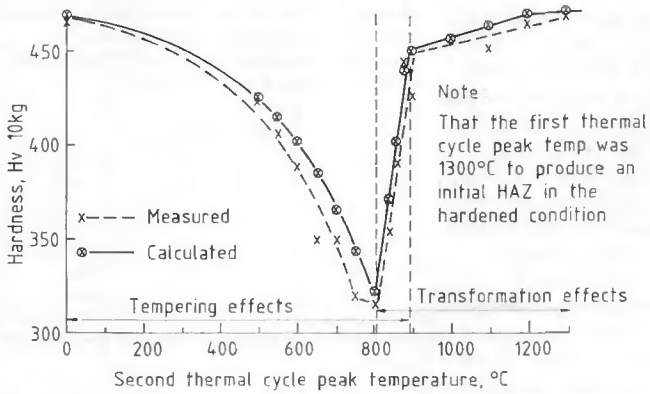

Fig. 8 – Calculated and measured hardness for weld simulated SA508 Class 2 HAZ's

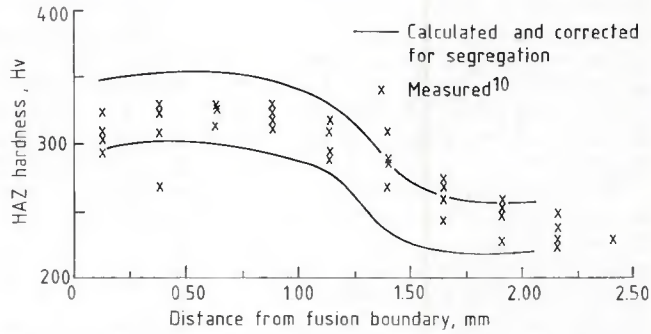

Fig. 9 – Calculated and measured as-welded HAZ hardness for a six-layer mechanized GTAW weld repair procedure (Ref. 10)

equal to the as-transformed hardness of those regions that experience a peak temperature equal to the Ac_3, *i.e.*, 449 Hv as described by Equation 9. That fraction of the HAZ that is not retransformed starts with an initial hardness appropriate to the particular condition produced by any transformation resulting from the preceding thermal history. This untransformed fraction of the HAZ is then tempered by the thermal cycle as described by Equations 12 to 14 as appropriate to the particular hardened condition.

The average HAZ hardness is then determined by the method of mixtures, *i.e.*

$$Hv = (\psi \times Hv^{New}) + (1 - \psi)(Hv^{Old}) \quad (18)$$

where ψ = fraction transformed

Hv^{New} = hardness of new transformation product

Hv^{Old} = hardness of old transformation product. Note that this is further tempered.

Validation of Transformation and Tempering Algorithms Using Weld Simulation Specimen Measurements

Prior sections describe a series of algorithms for the calculation of HAZ hardness as a result of retransformation, tempering and a combination of both. Clearly, there are many possible combinations for experimental validation, and so effort has been concentrated on the HAZ in the hardened condition since this condition represents the maximum HAZ hardness that will require softening during welding.

Table 8—Welding Conditions for Computer Model Validation

Welding Parameters	Layer Number 1	2	3-6
Current, A	180	200	220
Voltage, V	11	11	11
Travel Speed, mm/s	3.60	2.96	2.54
Wire Feed Speed, mm/s	16.5	25.0	27.5
Wire Diameter, mm	0.89	0.89	0.89
Preheat, °C	150	150	150

The combinations of weld thermal cycles used are given in Table 5, and the agreement between measured and calculated HAZ hardness produced by retransformation, temperature and a combination of both are shown in Fig. 8.

Figure 8 shows how an HAZ, which had initially experienced a weld thermal cycle peak temperature of 1316°C (2400°F), is affected by various second thermal cycles with peak temperatures in the range 20°-1300°C (68°-2372°F). Note that the first thermal cycle produces a HAZ in the hardened condition. Second thermal cycles with peak temperatures in the range 20°-808°C (68°-1456°F), *i.e.*, up to the Ac_1 temperature, temper the initial structure by various amounts producing a progressive decrease in hardness with peak temperature. The comparison of weld simulation hardness measurements and calculated hardness values derived from the algorithms expressed by Equations 6 to 17 show reasonable agreement.

For all second thermal cycle peak temperatures above 892°C (1608°F), the Ac_3 temperature, the structure is fully transformed, and since it previously experienced a thermal cycle peak temperature in excess of 1100°C, *i.e.*, 1300°C, the HAZ structure is also fully hardened. Consequently, the HAZ hardness produced by all those second thermal cycle peak temperatures above the Ac_3 are described by Equations 9 and 10. The resultant hardness changes are caused by transformation effects.

In the intermediate range of second thermal cycle peak temperatures, between the Ac_1 and Ac_3, hardness changes are caused by a combination of tempering and transformation effects, as described in a prior section.

Computer Model Validation

A series of five mechanized GTAW welding procedures identified by the computer model were validated experimentally (Ref. 10). The welding procedure detailed in Table 8 proved to be the most suitable for practical applications in cavity geometries. Hardness traverses for this procedure were calculated using the algorithms described previously using the computer model with randomized bead dimensions. The calculated maxima and minima from 150 independent hardness traverses across the HAZ are shown in Fig. 9, together with the measured hardness values taken from the separate traverses (Ref. 10).

The calculated and measured values for each of the five validated weld deposits were in reasonable agreement given the complexity of the situation and possible segregation in the base plate. The example given in Fig. 9 is typical.

Discussion

Weld Bead Dimensions

The computer model used requires suitable algorithms for the description of weld bead shape which has an idealized geometry as shown in Fig. 1. This has the disadvantage that the model is not generally applicable but is only valid over the range of conditions used to obtain the weld bead dimension data. In the present case, the database for weld bead dimensions is sparse. However, the computer model uses randomized weld bead data whose scatter is directly related to the scatter measured in the empirical database.

The computer model now has the capability to examine the effects of weld bead variability on a given weld. Since weld bead variability is the inherent source of weld variability, it allows the possibility to examine possible weld-to-weld variations, which could be important in some nuclear repair applications. This may help to define the level of experimental validation required to establish a given level of confidence that any given weld is adequately represented by a given set of test samples whose properties are well established. The agreement between the scatter of the hardness measurements and the band-

width of the calculated hardness maxima and minima envelopes (Fig. 9) indicates that the sparse weld bead dimension database used, together with the limited extrapolation in welding conditions, does not introduce any serious errors into the hardness calculations.

HAZ Dimensions

The HAZ dimensions are calculated using standard heat-flow equations. However, an average arc efficiency, η, has been used to constrain the calculations to fit the measured distance from the fusion boundary to the Ac_1 isotherm. Since the fusion boundary distance is determined empirically, adjusting η is equivalent to fitting the HAZ dimensions empirically. The heat-flow calculations are effectively calibrated against two fixed points in the HAZ, thereby overcoming most of the known limitations of classical heat flow. The alternative is to use a much more sophisticated finite element model that correctly models convective flow in the weld pool for a moving source with wire additions. At present, even the most sophisticated models cannot predict weld bead and HAZ dimensions from first principles (Refs. 11–17).

Computer Model Validation

Generally, the agreement between the measured and calculated hardness traverses is reasonable—Fig. 9. The band describing the hardness maxima and minima is in reasonable agreement with the measurements, given the coarseness of the algorithms derived from Fig. 7. In fact, the calculated shape fits the measured maximum HAZ hardness data points to within 10%. The discrepancy may be due to plate segregation (Ref. 10). For example, the specimens used to derive the tempering algorithms contained 0.39 wt-% Cr and 0.31 wt-% Si in contrast to the weld bead base plate and weld simulation specimens, which contained 0.28 wt-% Cr and 0.17 wt-% Si—Table 1. This composition difference can lead to hardness variations of about 20 Hv 10 kg (Refs. 18, 19).

In summary, therefore, the results demonstrate the feasibility of a welding technique where successive welding passes are used to control the HAZ structure and hardness. This provides some confidence that the structure and properties of the HAZ's of non-postweld heat treated weldments can be left in a softened metallurgical condition. The extensive program carried out by Babcock and Wilcox under the main EPRI contract RP 1236 has measured the mechanical properties of such repairs to underwrite the service integrity. However, it is unlikely that such techniques will have a major effect on the as-welded residual stress distribution and further work is required to assess the fitness for purpose of weld repair situations that do not involve postweld heat treatment.

Conclusions

1) The predictive methodology, in the form of a computer model, has the potential to be used for rapid weld evaluation of procedures and weld process parameter optimization.

2) A six-layer mechanized GTAW weld repair procedure, which uses the principles of layer-by-layer refinement and tempering during welding, has been identified as an acceptable alternative to the ASME XI half-bead technique.

3) Detailed hardness distributions across SA508 Class 2 heat-affected zones can be predicted for the mechanized GTAW process from a knowledge of the weld bead dimensions, welding process variables and basic heat-affected zone metallurgy.

References

1. Alberry, P. J., and Lambert, J. A. 1982. The welding metallurgy of SA508 Class 2 heat-affected zones. Int. Conf. on Welding Technology for Energy Applications, Session 5, Oak Ridge National Laboratory, Oak Ridge, Tenn.

2. Alberry, P. J., Brunnstrom, R. R. L., and Jones, K. E. 1983. Computer model for predicting heat-affected zone structures in mechanized tungsten inert gas weld deposits. *Metals Tech.* 10(1):28-38.

3. Myers, J. 1972. Weld simulation in a study of stress relief cracking in a CrMoV steel. Welding Institute Seminar on Weld Thermal Simulators for Research and Problem Solving.

4. Alberry, P. J., Chew, B. C., and Jones, W. K. C. Prior austenite grain growth in the heat-affected zone of a ½CrMoV steel. *Metals Tech.* 4(6):317–325.

5. Ikawa, H., Oshige, H., Noi, S., Date, H., and Uchikawa, K. 1978. Relation between welding conditions and grain size in weld heat-affected zone. *Trans. Jap. Weld. Soc.* 9(1):47–51.

6. Ashby, M. R., and Easterling, K. 1982. A first report on diagrams for grain growth in welds. *Acta Met.* 30(11):1969–1978.

7. Rosenthal, D. 1941. Mathematical theory of heat distribution during welding and cutting. *Welding Journal* 20(5):220-s to 234-s.

8. Christensen, N., Davies, V. L., and Gjermundsen, K. 1965. Distribution of temperatures in arc welding. *Brit. Weld J.* 12(2):54–75.

9. Hess, W. F., Merrill, L. L., Nippes, E. F., and Bunk, A. P. 1943. The measurements of cooling rates associated with arc welding and their application to the selection of optimum welding conditions. *Welding Journal* 22(9):377-s to 422-s.

10. Babcock and Wilcox. 1984. Repair welding of heavy section steel components in Light Water Reactors. EPRI NP-3614 Final Report, Project 1236-1.

11. Atthey, D. R. 1980. A mathematical model for fluid flow in a weld pool at high currents. *J. Fluid Mech.* 98:787.

12. Heiple, C. R., and Roper, J. R. 1982. Mechanism for minor element effect on GTA fusion zone geometry. *Welding Journal* 61(14):97-s to 102-s.

13. Fan, J., Tsai, C. L., and Baeslack, W. A. 1984. Modeling of transient weld pool behavior. 65th AWS Annual Meeting, Dallas, Tex., Session 15, Paper A.

14. Glickstein, S. S., and Friedman, E. 1984. Weld modeling applications. 65th AWS Annual Meeting, Dallas, Tex., Session 15, Paper B.

15. Glickstein S. S., and Friedman, E. 1981. Technical note: Effect of weld pool configuration on heat-affected zone shape. *Welding Journal* 60(6):110-s to 112-s.

16. Oreper, G. M., Eagar, T. W., and Szekely, J. 1983. Convection in arc weld pools. *Welding Journal* 62(11):307-s to 312-s.

17. Friedman, E. 1978. Analysis of weld puddle distortion and its effect on penetration. *Welding Journal* 57(6):161-s to 166-s.

18. Arata, Y., Nishiguchi, K., Ohji, T., and Kohsai, N. 1979. Weldability concept on hardness prediction. *Trans. J.W.R.I.* 8(1):43–52.

19. Boothby, P. J. 1982. Predicting hardness in steel HAZs. *Welding Institute Res. Bull.* (9):280–284.

Acknowledgments

The majority of this work was funded under EPRI contracts RP 1236-1 and RP 1757-28. Material was supplied by Babcock and Wilcox, Alliance, Ohio, under ERPI contract RP 1236-1. Helpful discussions with Mr. R. R. L. Brunnstrom (MEL), Mr. J. G. Feldstein (Babcock and Wilcox) and Dr. R. E. Nickell (EPRI) are gratefully acknowledged.

This paper is published by permission of the Electric Power Research Institute and the Central Electricity Generating Board, England.